



## Articles

### Optical Mapping in a New Guinea Pig Model of Ventricular Tachycardia Reveals Mechanisms for Multiple Wavelengths in a Single Reentrant Circuit

Steven D. Girouard, MS; Joseph M. Pastore, BS; Kenneth R. Laurita, MS; Kenton W. Gregory, MD; David S. Rosenbaum, MD

[+](#) Author Affiliations

Correspondence to David S. Rosenbaum, MD, Case Western Reserve University, Department of Biomedical Engineering, Wickenden Bldg, Room 504, Cleveland, OH 44106-7207. E-mail dsr@pace.cwru.edu.

#### Abstract

**Background** Although the relationship between cardiac wavelength ( $\lambda$ ) and path length importantly determines the stability of reentrant arrhythmias, the physiological determinants of  $\lambda$  are poorly understood. To investigate the cellular mechanisms that control  $\lambda$  during reentry, we developed an experimental system for continuously monitoring  $\lambda$  within a reentrant circuit with the use of voltage-sensitive dyes and a new guinea pig model of ventricular tachycardia (VT).

**Methods and Results** Action potentials were recorded simultaneously from 128 ventricular sites in Langendorff-perfused hearts ( $n=15$ ) in which propagation was confined to a two-dimensional rim of epicardium by an endocardial cryoablating procedure. The reentrant path was precisely controlled by creating an epicardial obstacle ( $2 \times 10$  mm) with an argon laser. To control for fiber orientation and rate-dependent membrane properties,  $\lambda$  during reentry was compared with  $\lambda$  during plane wave propagation transverse and longitudinal to cardiac fibers at a stimulus cycle length (CL) comparable to the VT CL. Reentrant VT (CL= $97.0 \pm 6.2$  ms) was reproducibly induced by programmed stimulation in 93% of preparations.  $\lambda$  varied considerably within the reentrant circuit (range, 10.6 to 22.5 mm), because of heterogeneities of conduction rather than action potential duration.  $\lambda$  was significantly shorter during reentrant propagation (ie, with pivoting) parallel to fibers ( $10.6 \pm 4.2$  mm) compared with plane wave propagation (ie, without pivoting) parallel to fibers ( $32.8 \pm 6.5$  mm,  $P < .02$ ), indicating that wave-front pivoting was primarily responsible for shortening of  $\lambda$  during reentry. The mechanism of  $\lambda$  shortening was conduction slowing from increased current load experienced by the pivoting wave front.

**Conclusions** We provide direct experimental evidence that multiple wavelengths are present even within a relatively simple reentrant circuit. Abrupt changes in loading during wave-front pivoting, rather than membrane ionic properties or fiber structure, were a major determinant of  $\lambda$  and, therefore, may play an important role in the stability of reentry.

#### Key Words:

[reentry](#)  
[tachycardia](#)  
[mapping](#)  
[action potentials](#)  
[electrophysiology](#)

The cardiac impulse was first described in terms of its  $\lambda$  by Mines in 1913, whose classic experiments led him to hypothesize that reentrant excitation is possible only if the reentrant path length is longer than the  $\lambda$  of the propagating impulse.<sup>1</sup> More recently, the concept of  $\lambda$  has been widely applied to the analysis of experimental<sup>2,3</sup> and theoretical<sup>4,5</sup> models of reentry, to the evaluation of antiarrhythmic drug mechanisms,<sup>6,7</sup> and to the clinical assessment of VT during electrophysiological testing.<sup>8</sup>

The  $\lambda$  hypothesis has been criticized because the reentrant wave is classically assumed to have constant length as it traverses the reentrant circuit; ie, a reentrant circuit is characterized by a single  $\lambda$ . Consequently, this description of  $\lambda$  fails to account for electrophysiological and structural heterogeneities known to exist within reentrant circuits.<sup>9,10</sup> Electrophysiological heterogeneities in ventricular myocardium may be caused by spatial dispersion of ionic membrane properties, which produces regional differences in APD and refractoriness.<sup>11,12</sup> Structural heterogeneities, such as tissue anisotropy<sup>13,14</sup> or changes in the geometry of a propagating reentrant wave front produced by conduction through a narrow isthmus,<sup>15,16,17</sup> or pivoting around obstacles<sup>18,19</sup> may introduce changes in conduction and refractoriness that are expected to additionally influence  $\lambda$ .

Due to limitations of conventional recording techniques, it has been difficult to simultaneously measure propagation, membrane repolarization, and details of wave-front geometry during reentrant excitation. Previously,  $\lambda$  has been estimated from the product of conduction velocity and refractoriness measured at a single recording site. An inherent limitation to this approach is that it cannot account for the presence of the aforementioned heterogeneities of conduction or refractoriness known to exist in reentrant circuits. Therefore, although  $\lambda$  is thought to underlie the functional characteristics and stability of most forms of reentry, it has been difficult to measure  $\lambda$  experimentally. Hence, the application of  $\lambda$  has

been largely restricted to one of a useful theoretical construct.

In our study, we applied high-resolution optical action potential mapping with voltage-sensitive dyes to a new intact guinea pig heart model of reentrant VT to investigate mechanisms of reentry at the cellular level. This approach allowed us to measure  $\lambda$  quantitatively in electrophysiologically and structurally heterogeneous tissue in which cardiac fiber orientation was known and the geometry of the circuit was precisely controlled with an argon laser. We provide experimental evidence demonstrating that  $\lambda$  cannot be assumed to be constant during reentry; instead multiple wavelengths exist in a single reentrant circuit. Moreover, the predominant mechanism responsible for heterogeneity of  $\lambda$  during reentry is conduction velocity slowing that resulted from the dissipation of excitatory current at the pivot points of the reentrant circuit rather than tissue anisotropy or heterogeneities of membrane repolarization.

## Methods

### Experimental Preparation

All experiments were carried out in accordance with the guidelines of the American Physiological Society. Retired male breeder guinea pigs weighing 750 to 1200 g were anesthetized intraperitoneally with 30 mg/kg sodium pentobarbital, and their hearts (weight, 3.1 to 4.2 g) were rapidly excised and perfused as Langendorff preparations with oxygenated (95% O<sub>2</sub>/5% CO<sub>2</sub>) Tyrode's solution containing (mmol/L): NaCl 130, NaHCO<sub>3</sub> 25, MgSO<sub>4</sub> 1.20, KCl 4.75, dextrose 5.0, and CaCl<sub>2</sub> 1.25 (pH 7.40, 37°C). Perfusion pressure was maintained at 80 mm Hg by adjusting the height of the perfusion reservoir relative to the height of the preparation. Hearts were stained with the voltage-sensitive dye di-4-ANEPPS (10  $\mu$ mol/L; Molecular Probes) by direct coronary perfusion for 5 minutes.

Beating and perfused hearts were immersed in a custom-built chamber made of acrylic plastic mounted onto a micromanipulator such that the mapping field could be positioned behind an imaging window located on the front of the chamber. Tyrode's solution in the chamber was maintained at 37°C with a heat exchanger to prevent intramyocardial temperature gradients. Gentle compression applied to the posterior surface of the heart with a movable piston was used to stabilize the anterior surface of the ventricle against the imaging window to ensure that the mapping surface and optical focal plane were coplanar, thus avoiding distortion of action potential signals. Previously, we have confirmed that this procedure does not alter the electrophysiological properties of this preparation.<sup>20 21</sup> Cardiac rhythm was monitored using three Ag/AgCl disk electrodes fixed to the chamber in positions corresponding to ECG limb leads I, II, and III. ECG signals were filtered (0.05 to 1000 Hz), amplified (1000 $\times$ ), and displayed on a digital oscilloscope (Gould DRO 1604). ECG tracings were printed on paper (100 mm/s) with a strip-chart recorder (Gould WindoGraf, model 40-8474).

### Experimental Model of Reentrant VT

To create essentially two-dimensional anisotropic myocardium free from the confounding influences of rotational anisotropy<sup>22</sup> or His-Purkinje breakthrough, a "frozen heart" preparation was created by ablating the endocardial three fourths of the LV wall using a modification of a cryoablation technique previously described in rabbits.<sup>23</sup> Langendorff-perfused hearts were immersed in a rapidly stirred, oxygenated, and temperature-controlled (30°C) Tyrode's bath. A cylindrical (4-mm diameter) brass tube, tapered at its tip to conform to the guinea pig LV apex, was then inserted through the mitral annulus into the LV. Coronary perfusion was interrupted for 7 minutes while liquid nitrogen (-196°C) was injected into the tube. To prevent reentry from occurring around the circumference of the heart,<sup>24</sup> the posterior RV was cryoablated transmurally. As a result of ablating the entire intraventricular septum, the endocardial and intramural layers of the LV, and the posterior RV, a thin (810 $\pm$ 220  $\mu$ m) viable rim of LV and anterior RV epicardia remained (Fig 1  $\Downarrow$ ). The electrophysiological properties of the viable epicardial rim were not altered by the cryoablation procedure, since conduction velocity, refractoriness, and action potential characteristics were found to remain normal in each preparation.

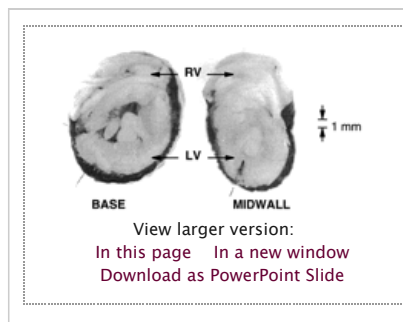


**Figure 1.**

Frozen heart preparation consisting of thin two-dimensional epicardial rim of viable myocardium. Shown are two cross sections parallel to the atrioventricular groove at the level of the ventricular base and midwall. The extent of myocardial necrosis is shown by triphenyl tetrazolium chloride staining.<sup>27</sup> The necrotic zone (light gray) extends from the LV endocardial wall through intramural layers up to a sharply demarcated viable epicardial rim (dark gray). To eliminate the possibility of reentry around the circumference of the heart,<sup>24</sup> the RV is completely ablated as well.

Previous investigators have created an anatomic obstacle for reentry by applying a cryoprobe to the epicardial surface of rabbit hearts.<sup>25 26</sup> In a series of pilot studies (unpublished observations), we found that epicardial cryoablation was not suitable for these studies since path length and geometry of the reentrant circuit could not be precisely controlled (eg, the area of necrosis was typically broad and irregular). Furthermore, since working distances are relatively small in the guinea pig, the epicardial cryoablation often impaired coronary blood flow, resulting in regional ischemia and depressed action potentials within the reentrant circuit. To circumvent these problems, we developed a system to produce epicardial reentry around an anatomic obstacle in which the geometry of the reentrant circuit is precisely controlled with a 5-W argon ion laser (model 2020-05, Spectra-Physics). Laser light was coupled into a 200- $\mu$ m diameter fiber-optic cable and focused (200  $\mu$ m spot) with a gradient index lens through the imaging window so that the obstacle could be "etched" onto the LV epicardium without moving the heart. A 2 $\times$ 10-mm linear obstacle (1-mm depth), oriented perpendicular to cardiac fibers and parallel to the left anterior descending coronary artery (Fig 2  $\Downarrow$ ), was created such that a thin zone of necrosis extended transmurally from the epicardial surface to the boundary of the endocardial cryoablation lesion. The position and translational velocity of the laser beam were precisely controlled ( $\pm$ 0.1  $\mu$ m) with three micropositioners (UT100-75, Klinger Corp) driven by a microprocessor with a software interface developed in our laboratory. The extent of the lesion was histologically confirmed after each experiment by 2,3,5-triphenyltetrazolium chloride staining<sup>27</sup> and light microscopy.

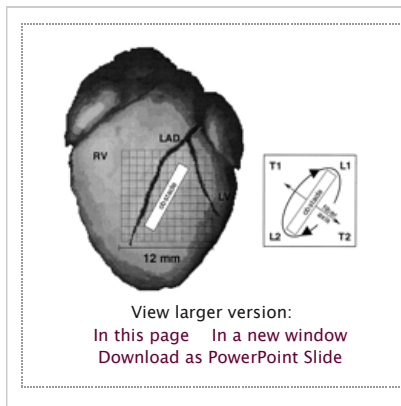


**Figure 2.**

Intact guinea pig heart preparation showing location of the 2×10 mm epicardial laser obstacle relative to the left anterior descending (LAD) coronary artery, anterior LV, and RV. Optical action potentials were recorded simultaneously from the mapping array (hatched area) that encompassed the entire reentrant circuit. Inset on the right shows the location of the reentrant path and obstacle relative to the cardiac fiber axis. APD, conduction velocity, and  $\lambda$  were compared in four predefined zones, (T1, T2, L1, and L2). These zones were based on the direction of reentrant propagation relative to fiber structure.

### Stimulation Protocol: Initiation of Sustained VT

The stimulation protocol was initiated no sooner than 30 minutes after completion of the cryoablation and laser ablation procedures to allow the preparation to equilibrate. Although these preparations exhibited stable action potential properties over the course of a 3-hour experiment, action potential maps reported in this study were recorded within 1 hour of establishing the Langendorff preparations. The epicardial surface was stimulated at 5× diastolic threshold current using a synthetic resin-coated (except at the tip) silver bipolar electrode (diameter, 0.1 mm; interelectrode spacing, 1 mm) and a programmable stimulator. We attempted to induce sustained monomorphic VT in 15 hearts using programmed ventricular stimulation. After a 10-beat constant CL drive train (CL=250 ms), single, double, and triple extrastimuli were introduced starting at 30 ms above the refractory period and then at intervals that scanned diastole by 5-ms decrements. When refractoriness to the last extrastimulus ( $S_N$ ) was reached, the  $S_{N-1}$  coupling interval was decreased by 5 ms and  $S_N$  was further decremented until refractoriness was again reached. If VT was not induced by extrastimulus technique, bursts of up to 25 consecutive stimuli were introduced. Every episode of VT was terminated with burst pacing and then reinitiated with programmed stimulation to confirm reproducibility of VT in this model.

### Stimulation Protocol: Plane Wave Stimulation

In five separate experiments, steady-state stimulation was carried out in the frozen heart preparation, without the epicardial obstacle, to investigate the dependence of  $\lambda$  on fiber orientation and rate in the absence of wave-front pivoting. With the use of a custom-built orthogonal plane wave electrode consisting of two bipolar pairs of platinum wires (0.5-mm diameter, 1-mm interelectrode spacing, 10-mm length) oriented perpendicular to one another, one electrode was used to stimulate a plane wave parallel to the cardiac fibers and the other stimulated a plane wave transverse to fibers. Action potentials were recorded from LV epicardium (Fig 2↑) during steady-state (>1 min) plane wave stimulation along one fiber axis at CLs ranging from 1000 to 100 ms. The identical stimulation protocol was repeated for plane wave propagation parallel and perpendicular to fibers.

### Optical Mapping With Voltage-Sensitive Dyes

We have developed an optical mapping system capable of recording high-fidelity action potentials simultaneously from 128 sites of an intact and beating heart (Fig 3↓). Voltage-sensitive dye was excited using quasimonochromatic light ( $540 \pm 10$  nm) from a 250-W tungsten-halogen lamp. Excitation light was directed toward the heart using a liquid light guide. Fluoresced and scattered light was collected using a high numerical aperture lens (50 mm, F1.8), long-pass filtered (610 nm), and focused onto a 12×12 element photodiode array (MD144-5T, Centronic Ltd). The camera design allowed optical magnification to be rapidly varied during an experiment. We used two magnifications in the present study. Low magnification (1.5×) yielded a 12×12-mm mapping area and 1.0-mm spatial resolution between recording pixels. High magnification (3.6×) yielded a 5×5-mm mapping area with 0.4-mm spatial resolution. A charge-coupled device video detector mounted coaxially on the camera housing was used to image the heart surface so that the mapping sites could be determined relative to the epicardial obstacle and coronary arteries. Photocurrent from each photodiode was converted to a voltage with the use of low-noise current-to-voltage amplifiers and then underwent postamplification (1×, 50×, 200×, and 1000×) with AC coupling ( $\tau=10$  s) and low-pass anti-alias filtering (1000 Hz). Action potential waveforms and ECGs were multiplexed and digitized directly to the disk of a UNIX workstation (Concurrent 5450S, Concurrent Computer Corp) with a 1-MHz 12-bit analog-to-digital converter at a sampling rate of 2000 Hz per channel (Fig 3↓).

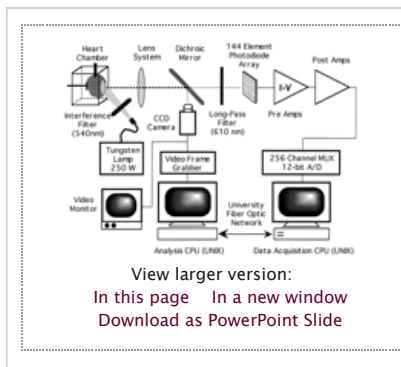


**Figure 3.**

Diagram shows optical mapping system used to record action potentials from the intact heart with high spatial (0.4 to 1.0 mm), temporal (0.5 ms), and voltage (1 mV) resolutions. See text for details.

This system was designed to optimize action potential fidelity to allow quantitative analysis of APD, conduction velocity, and  $\lambda$  in the intact heart. We have shown previously that optical action potentials recorded with this system closely mimic the time course and morphology of action potentials recorded with microelectrode techniques.<sup>20 28</sup> In these studies, action potentials could be recorded from the intact heart without motion artifact

because endocardial cryoablation anchored the epicardial surface and thus obviated the need for suppressing cardiac contraction with drugs known to influence action potential characteristics<sup>21 29</sup> and reentrant arrhythmias.<sup>30</sup> Action potentials were not distorted by this recording system since the bandwidth of the amplifiers was set well outside the frequency content of optical action potentials. The sampling rate used in these studies was approximately 10 times the highest frequency content of optical action potentials,<sup>20 28</sup> therefore cardiac action potentials could be accurately reconstructed from digitized waveforms. To optimize dynamic range, the large offset caused by background fluorescence of di-4-ANEPPS was removed without filtering out low-frequency components (eg, the plateau) of the action potential waveform by discharging the AC coupling capacitor just before each data acquisition. The high signal-to-noise ratio of the system made it possible to detect action potential amplitude changes as small as 1 mV (based on a 100-mV action potential).

### Measurement of Cardiac Wavelength From Optical Action Potential Maps

Optical action potentials were analyzed using a previously validated computer algorithm to automate the detection of activation and recovery times.<sup>31</sup> Activation time was defined as the point of maximum upstroke velocity, and recovery was defined as the point of maximum second derivative during repolarization. This corresponds to recovery measured at  $\approx 95\%$  repolarization<sup>32</sup> (ie, APD<sub>95%</sub>). All computer-assigned times were verified by the investigators.  $\lambda$  was determined from the product of mean APD and mean conduction velocity measured within the region of depolarized tissue such that  $\lambda$  was not dependent on APD or conduction velocity at any single point. For further confirmation,  $\lambda$  was also measured directly from isopotential maps as the extent of depolarized tissue (ie, distance from the depolarizing head of the wave to the point of recovery at the tail) surrounding the laser obstacle at any point in time.  $\lambda$  was not assumed to be stationary in time (ie, from beat to beat) or space (ie, throughout the reentrant circuit) but was measured as a continuously changing function of the cardiac cycle. For the purpose of statistical analysis, the VT circuit was divided into four zones (L1, L2, T1, and T2; Fig 2↑, inset) based on direction of reentrant propagation relative to the cardiac fiber orientation. Zones L1 and L2 were near pivot points of the circuit where the wave front turns in the longitudinal fiber direction. Zones T1 and T2 were located on either side of the long axis of the linear obstacle where propagation is transverse to cardiac fibers.

### Statistical Analysis

Statistical comparisons of APD, conduction velocity, and  $\lambda$  during plane wave propagation parallel and perpendicular to fibers were made using a Student's paired *t* test. APD, conduction velocity and  $\lambda$  in various zones (L1, L2, T1, and T2) of the reentrant circuit were also compared using a Student's *t* test. A value of  $P < .05$  was considered to be statistically significant, and a Bonferroni correction for multiple comparisons was applied when appropriate.

## Results

### Characteristics of Experimental VT Model

Computer-driven laser ablation proved effective for producing precisely controlled reentrant circuits. The dimensions of the epicardial obstacle were nearly identical in all experiments, resulting in a consistent reentrant path length (range, 23.0 to 26.5 mm). The epicardial obstacle had sharply demarcated borders as normal action potentials were recorded from sites as close as 400  $\mu\text{m}$  from the obstacle border.

Reentrant VT was initiated with programmed stimulation in 14 of 15 (93%) hearts (VT CL =  $97.0 \pm 6.2$  ms). In every experiment, VT was pace-terminated and reinitiated to ensure reproducibility of the model. In several cases, burst pacing at one CL produced classic entrainment of VT (in 8 of 14 experiments) or acceleration to polymorphic VT (in 2 of 14 experiments), while pacing at other CLs terminated VT. A reentrant mechanism was confirmed by direct action potential mapping of the entire circuit. Fig 4↓ illustrates a representative isochrone activation map of VT. Conduction proceeds clockwise around the linear obstacle, and conduction velocity is most rapid along the long axis of the lesion where propagation is transverse to myocardial fibers. In contrast, conduction slows near each pivot point where propagation turns parallel to fibers. Despite the relatively fast CL of VT, action potentials recorded from the reentrant circuit exhibited well-defined upstrokes, plateaus, repolarization, and diastolic intervals (Fig 4↓). In this model, VT remained stable and persisted for more than 2 hours unless actively terminated by pacing.

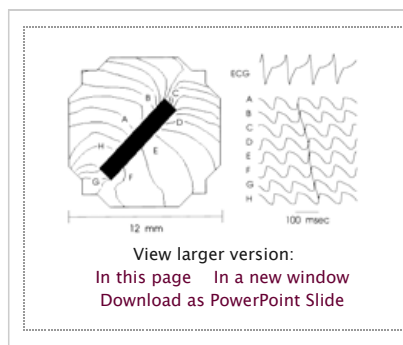


**Figure 4.**

Activation map (4-ms isochrones) during reentrant VT in the guinea pig model generated from 128 simultaneously recorded optical action potentials. Activation proceeds clockwise around the laser-induced epicardial obstacle (black area). In this case the reentrant path length was 25 mm long, and the VT CL was 98 ms. In the right panel, action potentials from representative sites around the circuit (A through H) are shown beneath an ECG. Arrows indicate the sequence of activation during VT.

### Cardiac Wavelength During Plane Wave Stimulation

To determine the dependence of  $\lambda$  on rate-dependent membrane properties and fiber orientation independent of the effects of pivoting,  $\lambda$  was measured during steady-state plane wave stimulation over a wide range of stimulus CLs. APD, conduction velocity, and  $\lambda$  are plotted in Fig 5↓ as a function of stimulus CL. APD decreased exponentially at faster CLs, but APD did not differ significantly during propagation longitudinally (Fig 5↓, filled circles) compared with transversely (Fig 5↓, open circles) to myocardial fibers. Conduction velocity also fell sharply at rapid CLs (<200 ms), but unlike APD, conduction velocity was significantly influenced by fiber direction. However, as stimulus CL approached 100 ms (ie, near the VT CL), the differences in conduction velocity between the two orthogonal fiber directions decreased owing to preferential conduction velocity slowing longitudinal to fibers (Fig 5↓). Due to these rate-dependent changes in conduction velocity, at relatively slow CLs there was a large difference in the magnitude of  $\lambda$  in the longitudinal and transverse directions (Fig 5↓,  $\lambda_L - \lambda_T \approx 40$  mm), whereas at rapid CLs fiber orientation had less influence on  $\lambda$ .

(Fig 5  $\Downarrow$ ,  $\lambda_L - \lambda_T \approx 10$  mm).

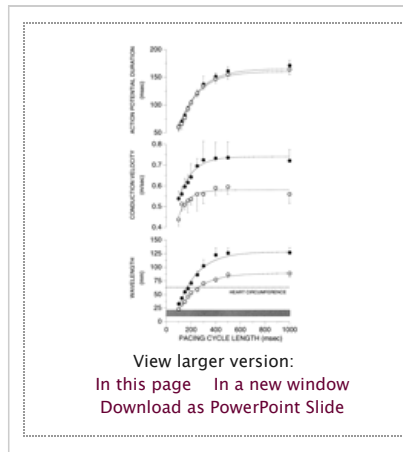


**Figure 5.**

Graph shows rate dependence of APD, conduction velocity, and  $\lambda$  in the frozen heart preparation consisting of a thin epicardial rim. Optical action potentials were recorded from 128 sites during steady-state plane wave stimulation parallel (-) and transverse (o) to cardiac fibers. Mean APD (top), conduction velocity (middle), and  $\lambda$  (bottom) measured for a broad range of cycle lengths (CL) are shown. At long CLs, comparable to normal guinea pig heart rate (CL >300 ms),  $\lambda$  is much longer than the heart circumference (dashed line). At rapid heart rates, however,  $\lambda$  shortens substantially, indicating that  $\lambda$  is highly sensitive to rate. Gray shaded box indicates range of  $\lambda$  observed during reentrant VT. Values shown are mean  $\pm$  SEM.

### Cardiac Wavelength During Reentry

In Fig 6  $\Downarrow$ , APD, conduction velocity, and  $\lambda$  measured during reentrant VT (shaded bars) are compared in four predefined zones (T1, T2, L1, and L2 in Fig 2  $\Uparrow$ ) of the circuit. To determine the influence of wave-front pivoting independent of fiber orientation and rate, Fig 6  $\Downarrow$  also shows  $\lambda$  measured during plane wave propagation longitudinal and transverse to cardiac fibers using a stimulus CL equivalent to the VT CL. During reentry, APD did not vary significantly around the circuit (Fig 6  $\Downarrow$ , left, compare L1, L2, T1, and T2) and was not significantly different from APD measured during plane wave stimulation (Fig 6  $\Downarrow$ , left, compare L1 and L2 to Lp). Although subtle variations of APD (typically <10 ms) were observed within the VT circuit, dispersion of APD did not contribute significantly to the heterogeneity of  $\lambda$ .

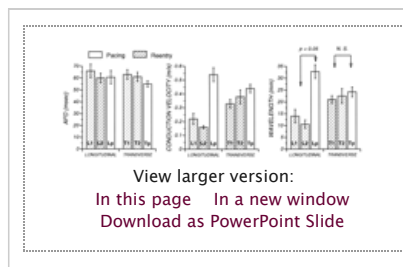


**Figure 6.**

Bar graphs show comparison of APD, conduction velocity, and  $\lambda$  measured in four zones (L1, L2, T1, and T2; see Fig 2  $\Uparrow$ ) of the reentrant circuit during reentrant VT (shaded bars). To control for the effects of rate-dependent membrane properties and fiber orientation, these values are compared during plane wave propagation (white bars) longitudinal (Lp) and transverse (Tp) to cardiac fibers while the preparation is paced at the VT CL. See text for details.

In contrast to APD, conduction velocity (Fig 6  $\Uparrow$ , center) differed markedly in the four zones of the circuit. During reentry, when propagation was transverse to cardiac fiber orientation (T1, T2), conduction was faster than in zones in which the wave front was pivoting parallel to fibers (L1, L2). In zones T1 and T2, velocity was not significantly different than would be expected from anisotropic conduction during plane wave stimulation (Fig 6  $\Uparrow$ , center, T1, T2  $\approx$  Tp). However, within zones L1 and L2, conduction velocity was significantly slower than would be expected from anisotropy (Fig 6  $\Uparrow$  center, L1, L2 < Lp). Consequently, the relation between longitudinal (L1, L2) and transverse (T1, T2) conduction velocities during reentrant propagation was reversed from their relationship during plane wave propagation.

With the use of optical action potential mapping, it was possible to measure  $\lambda$  directly by plotting the extent of depolarized tissue within the reentrant circuit at any time. The isopotential contour maps in Fig 7  $\Downarrow$  demonstrate how  $\lambda$  dynamically expands and contracts within a single reentrant VT cycle. These maps depict the voltage distribution in the reentrant circuit at two time points (A and B) separated by 27 ms. The white arrow in each map extends from the tail of recovery to the leading edge of depolarization and therefore corresponds to  $\lambda$ . At time A (Fig 7  $\Downarrow$ , left), the leading edge of depolarization has passed through an area of slow conduction around a pivot point; hence,  $\lambda$  contracts as the repolarizing tail of the wave front begins to “catch up” with the slowly propagating head. At time B (Fig 7  $\Downarrow$ , right), the leading edge has just conducted rapidly down the long axis of the obstacle; hence,  $\lambda$  expands. In these experiments,  $\lambda$  varied by 20% to 50% during an individual cycle of reentrant VT. Also note that there is corresponding variation of the “excitable gap” (Fig 7  $\Downarrow$ , black region) as indicated by changes in the area of fully repolarized tissue at time A versus time B. The pattern of  $\lambda$  changes during the VT cycle (Fig 7  $\Downarrow$ , inset) was identical from beat to beat.

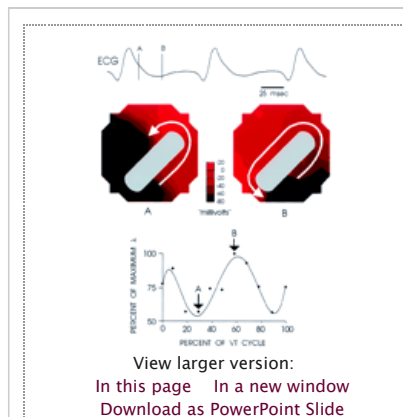


**Figure 7.**

Isopotential maps derived from high resolution optical action potential recordings demonstrate the heterogeneity of  $\lambda$  and excitable gap during a single reentrant VT cycle. Transmembrane potential was normalized at each recording site (-80 mV resting potential; +20 mV maximum amplitude) and the distribution of transmembrane potentials measured in the reentrant circuit are plotted for two points of time (A and B). Reentry proceeds counterclockwise around an epicardial obstacle (hatched area).  $\lambda$  is indicated by the white arrow that extends from the head to the tail of the wave front and corresponds to the extent of depolarized (inexcitable) tissue. Conversely, the excitable gap is depicted by the area of repolarized (excitable) tissue shown in black. At time A,  $\lambda$  comprised 48% of the circuit; whereas at time B,  $\lambda$  comprised 88% of the circuit. Inset demonstrates variations of  $\lambda$  during the entire reentrant VT cycle.

## Mechanism for Multiple Wavelengths During Reentry

We found that conduction velocity slowing near pivot points of the reentrant circuit was the most important factor that caused  $\lambda$  to vary during VT. To investigate the mechanisms of conduction velocity slowing, high-magnification action potential maps (400- $\mu\text{m}$  interpixel resolution) were recorded at each pivot point during reentrant VT and were compared with action potentials obtained from the similar site during plane wave propagation. An example of propagation around a pivot point is shown in Fig 8 $\downarrow$ . As the impulse begins to rotate, there is profound conduction slowing (ie, crowding of isochrones) at the pivot point fulcrum, whereas more rapid conduction occurs at sites distant from the pivoting fulcrum. As the wave front exits the pivot point, uniform conduction is restored across the wave front.

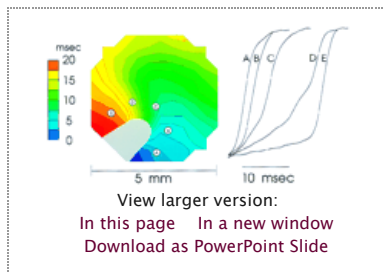


**Figure 8.**

High magnification map (400  $\mu\text{m}$  resolution) of depolarization (1-ms isochrones) around the basal tip of the epicardial obstacle (hatched area) during reentrant VT. Pivoting around the obstacle requires that the reentrant wave front first propagate transverse to fibers (blue region), then turn parallel to fibers (blue >green >yellow), and finally turn transverse to fibers again (red region). As the wave front pivots, conduction *slows* (ie, crowding of isochrones) paradoxically as propagation turns *parallel* to fibers. Action potential upstrokes recorded from five evenly spaced sites around the pivot point are shown to the right. While the wave front enters the pivot point (A, B) conduction is relatively fast and upstrokes are sharp. However, as the wave front pivots (C, D) action potential upstrokes become increasingly slowed. After pivoting is complete (E), conduction and action

potential upstroke velocity are again normal.

Alterations of conduction velocity were associated with marked slowing in the time course of action potential upstrokes at each pivot point. Action potential upstrokes recorded from five uniformly spaced sites around the pivot point are shown in Fig 8 $\uparrow$ . As the wave front approaches the pivot point, action potential upstroke velocity is rapid (Fig 8 $\uparrow$ , right, potentials A and B) and is no different than upstrokes observed in other nonpivoting areas of the circuit. However, as the propagating wave pivots, action potential upstrokes become progressively slowed and contain irregularities and multiple notches not observed at nonpivoting sites (Fig 8 $\uparrow$ , right, potentials C and D). During plane wave stimulation (ie, in the absence of pivoting), the potentials recorded from sites C and D exhibited normal upstrokes, indicating that action potential upstroke delays and conduction slowing during reentry were caused by altered loading of the pivoting wave front and not because these cells were intrinsically depressed or injured. Finally, upstroke slowing could not be attributed to artifactual blurring of optical action potentials within a recording pixel (see "Appendix").

To investigate the extent to which the natural isthmus formed by the AV groove and the basal tip of the laser lesion may affect conduction, an additional lesion was created using the argon laser in a stepwise fashion starting from the AV groove and extending toward the obstacle. Isthmus width was narrowed progressively during VT, and VT CL was measured as a function of isthmus width. Fig 9 $\downarrow$  shows that VT CL did not vary with decreasing isthmus width. In three hearts tested, there was no significant change in the VT CL until a critical width was reached, at which time VT terminated and could no longer be initiated. These data suggest that the isthmus width affected refractoriness without altering conduction velocity and hence was not expected to have influenced  $\lambda$  significantly during steady-state VT.

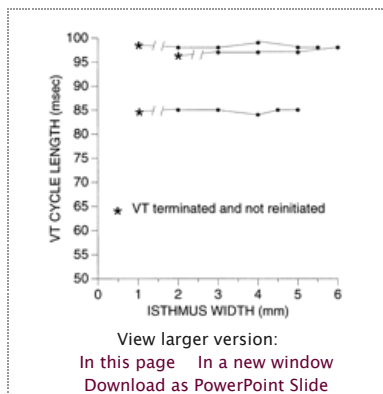


**Figure 9.**

The natural isthmus formed by the atrioventricular (AV) groove and the basal tip of the epicardial obstacle was progressively shortened by extending a laser lesion progressively downward from the AV groove toward the obstacle. Consequently, the reentrant circuit was forced to propagate through a progressively narrowed isthmus, and the VT CL was measured to determine whether conduction slowing around the pivot points could be explained by this isthmus. Isthmus width did not affect conduction as measured by VT CL. The isthmus became refractory when its width was reduced to 1 to 2 mm, resulting in termination of VT that could not be reinitiated.

## Discussion

A variety of experimental techniques have been used previously to investigate arrhythmia mechanisms, including multisite extracellular mapping and single-cell microelectrode and patch-clamp recordings. Extracellular techniques offer reasonable spatial resolution but limited information on the time course of membrane potential change. On the other hand, microelectrode and patch-clamp recordings provide detailed and quantitative information concerning membrane events but only from one cell. It has been suggested that "[an understanding of] the interaction of ionic currents and the means by which electrical activity is propagated between cells requires a more integrated approach."<sup>33</sup> Accordingly, in the present study, we used high-resolution optical action potential mapping to study reentry at the cellular level in the intact and beating heart.

Optical mapping provided direct experimental evidence that  $\lambda$  is not a static property of reentry; rather,  $\lambda$  varies continuously within a reentrant circuit. Although fiber structure and rate-dependent ionic membrane properties influenced  $\lambda$ , during established reentry these properties did not

cause heterogeneity of  $\lambda$  within the reentrant circuit. In contrast, we found that dissipation of excitatory current caused by changes in the geometry of the reentrant wave front at the pivot points of the circuit was primarily responsible for heterogeneity of  $\lambda$  observed during reentry.

### Characteristics of the Guinea Pig VT Model

We have developed a unique experimental system that allowed us to record high-fidelity action potentials from the intact heart and therefore to monitor  $\lambda$  continuously throughout the entire reentrant circuit. This was possible because our guinea pig model of VT was designed so that the reentrant circuit could be confined to essentially two dimensions, and the geometry of the reentrant path was precisely controlled with an argon ion laser. Conduction within the thin epicardial rim simulated chronic myocardial infarct models<sup>34</sup> while eliminating the confounding effects of ischemia<sup>35</sup> and nonuniform anisotropy.<sup>36</sup> Reentrant VT in this model shared many of the characteristics of clinically encountered VT. For example, VT was reproducibly initiated using a clinically relevant stimulation protocol and could be terminated, entrained, and accelerated with pacing. Although the VT CL was relatively fast, action potentials recorded during VT demonstrated sharp upstrokes and normal plateaus, indicating that reentry did not require the presence of depressed tissue within the circuit.

### Dependence of Wavelength on Rate-Dependent Membrane Properties and Fiber Structure

To date, cardiac  $\lambda$  has not been well characterized in ventricular myocardium. In the present study,  $\lambda$  measured during plane wave stimulation was dependent on both stimulation rate and fiber structure (Fig 5 [↑](#)). We found that  $\lambda$  shortened exponentially with increased stimulation frequency. This was an expected result since  $\lambda$  is dependent on conduction velocity and APD, both of which decrease at faster stimulation rates. Dynamic shortening of  $\lambda$  with increased rate has also been observed in rabbit<sup>2</sup> and canine<sup>37</sup> atria, reaffirming that  $\lambda$  is not a static property of cardiac muscle. Although fiber structure did not affect APD,  $\lambda$  was consistently longer during propagation in the longitudinal direction compared with the transverse direction due to anisotropic conduction. These data suggest that the  $\lambda$  of a propagating impulse adapts to the local electrophysiological environment and thus can contract or expand dynamically as conditions change.

Dynamic adaptation of  $\lambda$ , and specifically the capacity of  $\lambda$  to contract at rapid heart rates, was critical to the formation of reentrant VT in our model. As shown in Fig 5 [↑](#), at physiological heart rates (CL=300 to 400 ms)  $\lambda$  was much longer than the circumference of the entire heart. Therefore, reentry could not be initiated (since  $\lambda \gg$  path length) had  $\lambda$  not contracted to the dimensions of the reentrant circuit at more rapid CLs. Data presented in Fig 5 [↑](#) also provide insight into mechanisms that control  $\lambda$  during reentrant VT. If  $\lambda$  were governed exclusively by fiber orientation and the rate-dependent ionic processes that govern depolarization and repolarization, the  $\lambda$  observed during VT would be expected to be identical to  $\lambda$  measured during plane wave stimulation at the VT CL. This was not the case, because the range of  $\lambda$  observed during reentrant VT (Fig 5 [↑](#), shaded bar) was significantly less than  $\lambda$  measured during plane wave stimulation at the VT CL ( $\approx$ 100 ms). Therefore, the degree to which  $\lambda$  shortened during reentrant VT cannot be attributed to anisotropic conduction or rate-dependent changes in APD or conduction velocity but was explained by the presence of wave-front pivoting, since this was the only difference between reentrant propagation and plane wave propagation in these experiments. In fact, one would predict from Fig 5 [↑](#) that in the absence of pivoting (ie, during plane wave propagation),  $\lambda$  would be longer than the reentrant path length, thus precluding the initiation of reentry. Therefore, in this experimental model, pivoting was critical to the development of reentry.

### Multiple Wavelengths During Reentry

A major finding of this study was that even in a relatively simple reentrant circuit, and in the absence of regional tissue injury, the  $\lambda$  of a reentrant impulse varies considerably as it traverses a circuit. It should be emphasized that our result does not diminish the importance of  $\lambda$  to the mechanism of reentry. Rather, our data indicate that the relationship between  $\lambda$ , path length, and the stability of reentry is more complex than many earlier investigations suggested. This was predicted from recent computer simulations by Rudy,<sup>38</sup> who concluded that "one should use caution when using a single value of wavelength or excitable gap as an index of stability of reentry."

Reiter et al<sup>26</sup> estimated  $\lambda$  and excitable gap from four discrete zones of a reentrant circuit in rabbit ventricle and also found that  $\lambda$  and excitable gap varied throughout the circuit. Moreover, they found that conduction velocity varied by 66% (range, 20 to 59 cm/s), whereas refractoriness varied by  $\approx$ 12% throughout the reentrant circuit, supporting our finding that heterogeneous conduction influences regional changes in  $\lambda$  more than do heterogeneities of refractoriness or APD. It was somewhat surprising to find that membrane repolarization was so homogeneous during VT in our model, particularly since we previously observed considerable APD gradients in guinea pig epicardium at physiological heart rates,<sup>31</sup> and since there is ample evidence that ion channels that govern repolarization are heterogeneously distributed throughout the ventricle. However, regional variations in transient outward current<sup>39</sup> as well as variations in the components of delayed rectifier current,  $I_{Kr}$  and  $I_{Ks}$ ,<sup>40</sup> have been observed predominantly at slow heart rates and not during tachycardia; hence, variability in the activity of these currents may be more important to the initiation than maintenance of reentry.

Cardiac  $\lambda$  is classically described as a homogeneous property of a reentrant impulse such that a single  $\lambda$  characterizes an entire circuit.<sup>1 41 42</sup> Consequently, investigators have estimated  $\lambda$  from the product of conduction velocity and APD (or refractoriness) measured at a single recording site. An inherent limitation to this approach is that it assumes that electrophysiological properties, including  $\lambda$ , are homogeneous throughout the circuit. Our data demonstrate that this approach is oversimplified and is probably only valid under ideal conditions such as plane wave propagation in structurally and electrophysiologically homogeneous tissue. Investigators<sup>10 26</sup> have also used the local effective refractory period (ERP) to estimate  $\lambda$  (ie, the length of time myocardium at one site is refractory rather than the length of refractory tissue at any point in time) and similarly have estimated excitable gap by subtracting ERP from the tachycardia CL (ie, the length of time myocardium at one site is excitable rather than the length of excitable tissue at any point of time). Had we calculated  $\lambda$  and excitable gap in this manner, we would have failed to observe heterogeneities of  $\lambda$  and excitable gap during reentry, since APD was relatively homogeneous throughout the VT circuit. However, as shown in Fig 7 [↑](#), our direct measurement of  $\lambda$  as the extent of depolarized tissue in space revealed  $\approx$ 50% variation of  $\lambda$  during a single reentrant cycle. Although the results from our experimental model should be extrapolated cautiously to VT in patients, these findings may explain why responses of clinical VT to artificial stimulation (ie, entrainment, termination) are so highly dependent on the region of the reentrant circuit in which stimuli are delivered.<sup>43 44</sup>

A more complete description of  $\lambda$  and excitable gap requires that these parameters be viewed with regard to how they vary in both time and space. The  $\lambda$  of a reentrant impulse should be determined from the difference between conduction velocity at the head of the impulse and repolarization

velocity at the tail of the impulse. Whenever the head is propagating faster than the tail,  $\lambda$  will lengthen; conversely, when the velocity of the head is slower than the tail,  $\lambda$  will shorten. Since the depolarizing head and repolarizing tail of a reentrant wave front are located simultaneously in different regions of the circuit, and typically propagate at different velocities, it is not possible to accurately measure  $\lambda$  without measuring conduction and repolarization at the head and tail of the impulse simultaneously. Spinelli and Hoffman<sup>10</sup> have previously emphasized the limitations of measuring  $\lambda$  from a single recording site. In contrast to optical action potential maps in which APD can be monitored continuously over time from multiple sites in space, ERP is measured from one site during a relatively long period of time. Therefore, it is not possible to monitor  $\lambda$  using extracellular techniques during important transient events such as the initiation and termination of reentry. Techniques similar to those used in this study may also help to elucidate the role of  $\lambda$  in the mechanism of drug-induced termination of reentry.

### Mechanisms of Wavelength Heterogeneity and the Role of Wave-Front Pivoting

All forms of reentrant excitation, whether due to functional<sup>42 45</sup> or anatomic<sup>46</sup> block or tissue anisotropy,<sup>47</sup> require that wave fronts rotate and pivot so that a complete circuit is established. Little information is available on the electrophysiological effects of wave-front pivoting and their relationship to the geometry of reentrant circuits. Heterogeneity of  $\lambda$  in our experimental VT model was primarily due to conduction slowing at the pivot points of the reentrant circuit rather than regional heterogeneities of membrane repolarization or anisotropic fiber structure. During plane wave propagation, action potential characteristics were normal at pivot points, ruling out the possibility that this tissue was intrinsically depressed. In contrast, during VT, action potentials (Fig 8↑, right) exhibited markedly slowed upstrokes close to but not remote from the pivoting fulcrum, indicating that conduction slowing at the pivoting fulcrum was related to the curvature of the rotating wave front. This can be explained by increased current load, as the excitatory current of a curved wave front is dissipated over a larger cross-sectional area producing a current sink.<sup>17 38</sup> Experimental<sup>13 48</sup> and computer modeling<sup>5</sup> studies have confirmed that an abrupt increase in axial current load produced by branching points or a sudden change in the direction of propagation will impair conduction. Also consistent with this mechanism is the fact that conduction slowing could not be explained by rate-dependent membrane properties, fiber structure (Fig 5↑, center), local prolongation of APD at the pivot points (Fig 6↑, left), or conduction through an isthmus (Fig 9↑).

The fact that conduction was *slowest* at the pivot points at which propagation turned *parallel* to cardiac fibers indicates that the influence of pivoting on conduction was far stronger than the influence of anisotropy. This apparent paradox can also be explained on the basis of source-sink relationships at the pivot points of the reentrant circuit. Pivoting from the transverse to the longitudinal fiber direction results in an abrupt change in the electrotonic load experienced by cells at the pivoting fulcrum. As the wave front turns, there is increased current load owing to reduced axial resistance in the longitudinal direction. Thus, tissue anisotropy may have created an additional current sink that further depressed conduction of the pivoting wave front. It is not possible from our data to distinguish the relative contributions of wave-front curvature and tissue anisotropy to altered current loading at the pivot points. However, previous experimental studies have demonstrated that a close, inverse correlation exists between the curvature of a pivoting wave front and local membrane response<sup>17</sup> and that these source-sink changes are not dependent on a specific fiber orientation.<sup>49</sup>

Pivoting may influence the stability of reentry in two opposing ways. In our experimental model, conduction slowing at the pivot points shortened  $\lambda$  sufficiently to prevent the head of the reentrant impulse from colliding with its tail, thus allowing stable reentry to persist. On the other hand, pivoting may produce a “weak link” in the reentrant circuit by imposing a local current load that may cause propagation to fail. This may be an important mechanism of arrhythmia termination in circumstances in which the reentrant path length is much longer than  $\lambda$  and in which head-tail interactions are less likely to occur. For example, during functional reentry in the sterile pericarditis model of atrial flutter, the pivot points of the reentrant circuit are consistently the sites of slow conduction and termination of reentry by either antiarrhythmic drugs or pacing.<sup>18</sup> These findings support the notion that the pivot point of a circuit can be a site of impaired propagation of excitatory current and therefore the component of the circuit that is most susceptible to the actions of antiarrhythmic drugs that depress excitability.

### Study Limitations

Multisite high-resolution action potential recordings made with voltage-sensitive dyes were critical to the measurement of  $\lambda$  in this study. The basis for our measurement of  $\lambda$  lies in the close quantitative relation between APD and refractory period.<sup>32 50</sup> Measurement of APD near complete repolarization, as used in this study, has been shown to closely parallel changes in refractoriness of ventricular myocardium.<sup>32</sup> This relation may not hold in slow fibers (eg, nodal cells) and in ischemic myocardium in which membrane recovery may outlast repolarization.<sup>51 52</sup>

Unlike reentrant VT in chronically healed myocardial infarction, our VT model is relatively simple. We made no attempt to incorporate several factors that may have an important influence on the arrhythmogenic substrate in patients, such as sympathetic stimulation,<sup>53</sup> nonuniform anisotropy,<sup>36</sup> and endocardial-to-epicardial heterogeneities of repolarizing currents.<sup>11 54</sup> Our experimental model was intentionally designed to eliminate these confounding influences so that it would be possible to study the independent effects of fiber orientation, circuit geometry, and membrane repolarization on  $\lambda$  in a controlled fashion. The effects of wave-front pivoting may be even more important in reentrant VT after myocardial infarction in which the reentrant path is tortuous and includes multiple pivot points. Further studies of experimental systems such as ours that also incorporate these additional complexities are required to provide a more complete understanding of the mechanisms of VT in humans.

### Selected Abbreviations and Acronyms

APD=action potential duration  
CL =cycle length  
 $\lambda$  =wavelength  
LV =left ventricular  
RV =right ventricle/right ventricular  
VT =ventricular tachycardia

### Appendix

Since an optical action potential arises from an average of single cell potentials within a recording pixel, prolongation of optical action potential upstroke rise time can theoretically be caused by conduction slowing (ie, "blurring" of the upstroke within a pixel) and may not necessarily indicate depressed excitability or altered loading at the level of the single cell. To rule out this possibility, one can express the rise time measured from an optical action potential upstroke ( $RT_{op}$ ) in terms of the single-cell rise time ( $RT_{cell}$ ) and the conduction velocity ( $\theta$ ) at a recording pixel of length ( $l$ ) as follows:

$$RT_{op} = RT_{cell} + \frac{l}{\theta}$$

Therefore, the single-cell rise time can be estimated from

$$RT_{cell} = RT_{op} - \frac{l}{\theta}$$

The  $RT_{op}$  measured at the pivot point of the reentrant circuit (eg, site D in Fig 8<sup>†</sup>,  $RT_{op}$ =14.5 ms) thus corresponds to a single-cell rise time,  $RT_{cell}$ =10 ms, which is substantially longer than  $RT_{cell}$  measured at nonpivoting sites (eg, site A in Fig 8<sup>†</sup>,  $RT_{cell}$ =2.0 ms). Therefore, the upstroke slowing observed at the pivot points was not an artifact of the optical recording technique but indeed represented the membrane response at the level of the single cell.

## Acknowledgments

---

This work was supported by NIH grant HL-54807, the Whitaker Foundation, the Medical Research Service of the Department of Veterans Affairs, and a Grant-in-Aid from the American Heart Association, Northeast Ohio Affiliate. The authors thank Mark Cohen, MD, for his assistance with the preparation and interpretation of the histological specimens. Also, we thank M.A. Allesie, MD, for his helpful suggestions in the development of the guinea pig VT model.

## Footnotes

---

Presented in part at the North American Society of Pacing and Electrophysiology Young Investigator Awards, May 6, 1995, Boston, Mass, and published in abstract form (*Pace*. 1995;18[pt II]:II-858).

Received June 19, 1995.

Revision received September 1, 1995.

Accepted September 11, 1995.

Copyright © 1996 by American Heart Association

## References

---

1. Mines GR. On dynamic equilibrium in the heart. *J Physiol (Lond)*. 1913;46:349-383.
2. Smoets J, Allesie MA, Lammer W, Benke F, Haller J. The wavelength of the cardiac impulse and reentrant arrhythmias in isolated rabbit atrium: the role of heart rate, autonomic transmitters, temperature, and potassium. *Circ Res*. 1986;58:96-108. [Abstract/FREE Full Text](#)
3. Frame LH, Simon M. Oscillations of conduction, action potential duration, and refractoriness: a mechanism of spontaneous termination of reentrant tachycardias. *Circulation*. 1988;78:1277-1287. [Abstract/FREE Full Text](#)
4. Coustamanche M, Glass L, Keener J. Instabilities of a propagating pulse in a ring of excitable media. *Physical Review Letters*. 1993;70:2178. [CrossRef](#) [Medline](#)
5. Quan W, Rudy Y. Unidirectional block and reentry of cardiac excitation: a model study. *Circ Res*. 1990;66:367-382. [Abstract/FREE Full Text](#)
6. Lewis T. *Mechanisms and Graphic Registration of the Heart Beat*. 3rd ed. London: Shaw & Son; 1925.
7. Boersma J, Bayazitov I, Abdallah H, Kirchhof S, Allesie M. Effects of bupropion, class Ia, and class III drugs on reentrant ventricular tachycardia: importance of the excitable gap for the inducibility of double-wave reentry. *Circulation*. 1994;90:1012-1022. [Abstract/FREE Full Text](#)
8. Callens DJ, Hoek BC, Jacobson MF. Comparison of resetting and entrainment of uniform sustained ventricular tachycardia: further insights into the characteristics of the excitable gap. *Circulation*. 1993;87:1229-1238. [Abstract/FREE Full Text](#)
9. Frame LH, Hoffman BF. Mechanisms of tachycardia. In: Surawicz B, Reddy CP, Prystowsky EN, eds. *Tachycardias*. Hague, the Netherlands: Martinus Nijhoff; 1984:276-301.
10. Spinelli W, Hoffman BF. Mechanisms of termination of reentrant atrial arrhythmias by class I and class III antiarrhythmic agents. *Circ Res*. 1989;65:1565-1579. [Abstract/FREE Full Text](#)
11. Antzelevitch C, Sicouri S, Litovsky SH, Lukas A, Krishnan SC, Di Diego JM, Cointant CA, Liu D. Heterogeneity within the ventricular wall: electrophysiology and pharmacology of epicardial, endocardial, and M cells. *Circ Res*. 1991;69:1427-1449. [FREE Full Text](#)
12. Fuzikawa T, Kimura S, Fuzikawa N, Bassett A, Muehrberg R. Potassium rectifier currents differ in myocytes of endocardial and epicardial origin. *Circ Res*. 1992;70:91-103. [Abstract/FREE Full Text](#)
13. Sacher W, Miller W, Cooley D, Parr R, Kootsey J, Johnson E. The discontinuous nature of propagation in normal canine cardiac muscle. *Circ Res*. 1981;48:39-54. [FREE Full Text](#)
14. Lammer W, Wit AL, Allesie MA. Effects of anisotropy on functional reentrant circuits: preliminary results of computer simulation studies. In: Sideman S, Boyer B, eds. *Activation, Metabolism, and Perfusion of the Heart: Simulation and Experimental Models*. Hague, the Netherlands: Martinus Nijhoff; 1987:133-149.

15. Isobe H, Zipes DP. Conduction over an isthmus of atrial myocardium in-vivo: a possible model of Wolff-Parkinson-White syndrome. *Circulation*. 1987;76:637-647. [Abstract/FREE Full Text](#)
16. Garrey W. The nature of fibrillary contraction of the heart: its relation to tissue mass and form. *Am J Physiol*. 1914;33:397-414.
17. Cabo C, Brette A-M, Brette WT, Davidenko IM, Gray RA, Jalife J. Wave-front curvature as a cause of slow conduction and block in isolated cardiac muscle. *Circ Res*. 1994;75:1014-1028. [Abstract/FREE Full Text](#)
18. Niwaya S, Ortiz L, Abo H, Gonzalez Y, Rudy Y, Waldo AL. Characterization of the excitable gap in a functionally determined reentrant circuit: studies in the sterile pericarditis model of atrial flutter. *Circulation*. 1994;90:1997-2014. [Abstract/FREE Full Text](#)
19. Agladze K, Keener JP, Muller SC, Panfilov A. Rotating spiral waves created by geometry. *Science*. 1994;264:1746-1748. [Abstract/FREE Full Text](#)
20. Girouard SD, Laurita KB, Rosenbaum DS. Unique characteristics of optically recorded action potentials. *Clinical Applications of Modern Imaging Technology II SPIE*. 1994;2132:347-357.
21. Girouard S, Laurita K, Rosenbaum DS. Optical mapping can resolve propagation and recovery in the intact beating heart. *PACE*. 1993;16(pt II):II-104. Abstract.
22. Colli Franzone B, Guerri I, Taccardi B. Potential distributions generated by point stimulation in a myocardial volume: simulation studies in a model of anisotropic ventricular muscle. *J Cardiovasc Electrophysiol*. 1993;4:438-458. [Medline](#)
23. Allegria MA, Schali M, Kirchhof CJH, Boersma J, Huybers M, Hollen J. Experimental electrophysiology and arrhythmogenicity: anisotropy and ventricular tachycardia. *Eur Heart J*. 1989;10:E2-E8.
24. Nattel S, Dillon SM, Bevilacqua S, Wit AL. Reentrant circuits and the effects of beta-blockers in a rabbit model of infarction with uniform anisotropic epicardial border zone. *J Cardiovasc Electrophysiol*. 1993;4:112-133. [Medline](#)
25. Brugada J, Boersma J, Abdallah H, Kirchhof C, Allegria M. Early wave termination of ventricular tachycardia: a common mechanism of termination of reentrant arrhythmias by various pharmacological interventions. *Circulation*. 1992;85:1879-1887. [Abstract/FREE Full Text](#)
26. Brette WT, Zolotarev Z, Kirchhof CJ, Boersma J, Allegria MA. Interaction of acute ventricular dilatation and d-sotalol during sustained reentrant ventricular tachycardia around a fixed obstacle. *Circulation*. 1994;89:423-431. [Abstract/FREE Full Text](#)
27. Fishbein MC, Meerbaum S, Bit L. Early phase acute myocardial infarct size quantification: validation of the triphenyl tetrazolium chloride tissue enzyme staining technique. *Am Heart J*. 1981;101:593-600. [CrossRef](#) [Medline](#)
28. Girouard SD. Design and validation of a high resolution cardiac action potential mapping system using voltage-sensitive dyes. Cleveland, OH: Case Western Reserve University, Department of Biomedical Engineering, 1993. Master's Thesis.
29. Liu Y, Cabo C, Salamez B, Delmar M, Davidenko I, Jalife J. Effects of diacetyl monoxime on the electrical properties of sheep and guinea pig ventricular muscle. *Cardiovasc Res*. 1993;27:1991-1997. [Abstract/FREE Full Text](#)
30. Taylor C, Amara A, Miles K, Kruthamer V, Jones J. Effects of diacetyl monoxime on cardiac action potential duration and fibrillation cycle length. *PACE*. 1994;17(pt II):II-824. Abstract.
31. Rosenbaum DS, Karlan DT, Kanti A, Jackson L, Coran H, Cohen BI, Salama G. Repolarization inhomogeneities in ventricular myocardium change dynamically with abrupt cycle length shortening. *Circulation*. 1991;84:1333-1345. [Abstract/FREE Full Text](#)
32. Efremov JB, Huang DT, Bond JM, Salama G. Optical mapping of repolarization and refractoriness from intact hearts. *Circulation*. 1994;90:1469-1480. [Abstract/FREE Full Text](#)
33. El-Sherif N. Experimental models of reentry, antiarrhythmic, and proarrhythmic actions of drugs: complexities galore. *Circulation*. 1991;84:1871-1875. [FREE Full Text](#)
34. Wit AL, Allegria M, Benke F, Lammers W, Smoots J, Franconi J. Electrophysiological mapping to determine the mechanism of experimental ventricular tachycardia initiated by premature impulses. *Am J Cardiol*. 1982;49:166-185. [CrossRef](#) [Medline](#)
35. Jones M, Klaber A. Electrophysiological changes and ventricular arrhythmias in the early phase of regional myocardial ischemia. *Circ Res*. 1981;49:1070-1081.
36. Spach MS, Josephson ME. Initiating reentry: the role of nonuniform anisotropy in small circuits. *J Cardiovasc Electrophysiol*. 1994;5:182-209. [Medline](#)
37. Boersma J, Allegria MA, Lammers WJFB, Benke FJM, Schali M. Length of excitation wave and susceptibility to reentrant atrial arrhythmias in normal conscious dogs. *Circ Res*. 1988;62:395-410. [Abstract/FREE Full Text](#)
38. Rudy Y. Reentry: insights from theoretical simulations in a fixed pathway. *J Cardiovasc Electrophysiol*. 1995;6:294-312. [Medline](#)
39. Liu D, W, Ciment CA, Antzelevitch C. Ionic bases for electrophysiological distinctions among epicardial, midmyocardial, and endocardial myocytes from the free wall of the canine left ventricle. *Circ Res*. 1993;72:671-687. [Abstract/FREE Full Text](#)
40. Liu D, W, Antzelevitch C. Characteristics of the delayed rectifier current (I<sub>Kr</sub> and I<sub>Ks</sub>) in canine ventricular epicardial, midmyocardial, and endocardial myocytes. *Circ Res*. 1995;76:351-365. [Abstract/FREE Full Text](#)
41. Winsor N, Rosenbluth A. The mathematical formulation of the problem of conduction of impulses in a network of connected excitable elements, specifically in cardiac muscle. *Arch Inst Cardiol Mex*. 1946;16:205-265. [Medline](#)
42. Allegria A, Benke JE, Schoerman EIC. Circus movement in rabbit atrial muscle as a mechanism of tachycardia: the role of nonuniform recovery of excitability in the occurrence of unidirectional block as studied with multiple microelectrodes. *Circ Res*. 1976;39:169-177.
43. Wallace HL, Dixon DP, Liu KI. Observations on mechanisms of ventricular tachycardia in man. *Circulation*. 1976;54:237-244. [Abstract/FREE Full Text](#)
44. Josephson ME, Horowitz LN, Farshidi A, Kastor JA. Recurrent sustained ventricular tachycardia, 1: mechanisms. *Circulation*. 1978;57:431-440. [Abstract/FREE Full Text](#)
45. Page PL, Plumb VJ, Okumura K, Waldo AL. A new model of atrial flutter. *J Am Coll Cardiol*. 1986;8:872-879. [Abstract](#)
46. Brugada J, Boersma J, Kirchhof C, Huybers M, Allegria M. Reentrant excitation around a fixed obstacle in uniform anisotropic ventricular myocardium. *Circulation*. 1991;84:1296-1306. [Abstract/FREE Full Text](#)
47. Spach M. Anisotropic structural complexities in the genesis of reentrant arrhythmias. *Circulation*. 1991;84:1447-1449. [FREE Full Text](#)
48. Spach M, Miller W, Jones F, Warren B, Barr B. Extracellular potentials related to intracellular action potentials during impulse conduction in anisotropic canine cardiac muscle. *Circ Res*. 1979;45:188-204. [Abstract/FREE Full Text](#)

49. Fast VG, Klaber AG. Cardiac tissue geometry as a determinant of unidirectional block: assessment of microscopic excitation spread by optical mapping in patterned cell cultures and in a computer model. *Cardiovasc Res.* 1995;29:697–707. [CrossRef](#) [Medline](#)
50. Franz M, Costard A. Frequency-dependent effects of quinidine on the relationship between action potential duration and refractoriness in the canine heart in situ. *Circulation.* 1988;77:1177–1184. [Abstract/FREE Full Text](#)
51. Boyett MR, Jewell PR. Analysis of the effects of changes in rate and rhythm upon electrical activity in the heart. *Prog Biophys Mol Biol.* 1980;36:1–52. [Medline](#)
52. Deussen F, Jasse M, Durrer D. The effect of acute coronary artery occlusion on subepicardial transmembrane potentials in the intact heart. *Circulation.* 1977;56:217–224. [Abstract/FREE Full Text](#)
53. Zipes DP, Mizazaki T. The autonomic nervous system and the heart: basis for understanding interactions and effects on arrhythmia development. In: Zipes DP, Jalife J, eds. *Cardiac Electrophysiology: From Cell to Bedside*. Philadelphia, Pa: WB Saunders Co; 1990:312–330.
54. Kramer I, Saffitz J, Wilkowitz E, Cox D. Intramural reentry as a mechanism of ventricular tachycardia during evolving canine myocardial infarction. *Circ Res.* 1985;56:736–754. [Abstract/FREE Full Text](#)

---

## Articles citing this article

### Optical Imaging of Voltage and Calcium in Cardiac Cells & Tissues

*Circ. Res.*, 2012;110:609–623,

[Abstract](#) [Full Text](#) [PDF](#)

### Interstitial volume modulates the conduction velocity–gap junction relationship

*Am. J. Physiol. Heart Circ. Physiol.*, 2012;302:H278–H286,

[Abstract](#) [Full Text](#) [PDF](#)

### Anisotropy of wave propagation in the heart can be modeled by a Riemannian electrophysiological metric

*Proc. Natl. Acad. Sci. USA.* 2010;107:15063–15068,

[Abstract](#) [Full Text](#) [PDF](#)

### Electromechanical wavebreak in a model of the human left ventricle

*Am. J. Physiol. Heart Circ. Physiol.*, 2010;299:H134–H143,

[Abstract](#) [Full Text](#) [PDF](#)

### A computational study of mother rotor VF in the human ventricles

*Am. J. Physiol. Heart Circ. Physiol.*, 2009;296:H370–H379,

[Abstract](#) [Full Text](#) [PDF](#)

### Mechanisms underlying increased right ventricular conduction sensitivity to flecainide challenge

*Cardiovasc Res.* 2008;77:749–756,

[Abstract](#) [Full Text](#) [PDF](#)

### Effect of heterogeneous APD restitution on VF organization in a model of the human ventricles

*Am. J. Physiol. Heart Circ. Physiol.*, 2008;294:H764–H774,

[Abstract](#) [Full Text](#) [PDF](#)

### Mechanoelectrical Feedback as Novel Mechanism of Cardiac Electrical Remodeling

*Circulation.* 2007;115:3145–3155,

[Abstract](#) [Full Text](#) [PDF](#)

### Dynamic changes of cardiac conduction during rapid pacing

*Am. J. Physiol. Heart Circ. Physiol.*, 2007;292:H1796–H1811,

[Abstract](#) [Full Text](#) [PDF](#)

### Matrix Metalloproteinase–7 Affects Connexin–43 Levels, Electrical Conduction, and Survival After Myocardial Infarction

*Circulation.* 2006;113:2919–2928,

[Abstract](#) [Full Text](#) [PDF](#)

### Phospholamban phosphorylation sites enhance the recovery of intracellular Ca<sup>2+</sup> after perfusion arrest in isolated, perfused mouse heart

*Cardiovasc Res.* 2006;70:335–345,

[Abstract](#) [Full Text](#) [PDF](#)

**Structure-Related Initiation of Reentry by Rapid Pacing in Monolayers of Cardiac Cells**

Circ. Res.. 2006;98:e29-e38,

[Abstract](#) | [Full Text](#) | [PDF](#)

**Optical mapping of late myocardial infarction in rats**

Am. J. Physiol. Heart Circ. Physiol.. 2006;290:H1298-H1306,

[Abstract](#) | [Full Text](#) | [PDF](#)

**Optical Imaging of the Heart**

Circ. Res.. 2004;95:21-33,

[Abstract](#) | [Full Text](#) | [PDF](#)

**Electrotonic load triggers remodeling of repolarizing current Ito in ventricle**

Am. J. Physiol. Heart Circ. Physiol.. 2004;286:H1901-H1909,

[Abstract](#) | [Full Text](#) | [PDF](#)

**Basic Mechanisms of Cardiac Impulse Propagation and Associated Arrhythmias**

Physiol. Rev.. 2004;84:431-488,

[Abstract](#) | [Full Text](#) | [PDF](#)

**A model for human ventricular tissue**

Am. J. Physiol. Heart Circ. Physiol.. 2004;286:H1573-H1589,

[Abstract](#) | [Full Text](#) | [PDF](#)

**Hysteresis Effect Implicates Calcium Cycling as a Mechanism of Repolarization Alternans**

Circulation. 2003;108:2704-2709,

[Abstract](#) | [Full Text](#) | [PDF](#)

**Transmural Electrophysiological Heterogeneities Underlying Arrhythmogenesis in Heart Failure**

Circ. Res.. 2003;93:638-645,

[Abstract](#) | [Full Text](#) | [PDF](#)

**Cardiomyocyte Cultures With Controlled Macroscopic Anisotropy: A Model for Functional Electrophysiological Studies of Cardiac Muscle**

Circ. Res.. 2002;91:e45-e54,

[Abstract](#) | [Full Text](#) | [PDF](#)

**Gap Junction Blockers Decrease Defibrillation Thresholds Without Changes in Ventricular Refractoriness in Isolated Rabbit Hearts**

Circulation. 2001;104:1544-1549,

[Abstract](#) | [Full Text](#) | [PDF](#)

**High resolution optical mapping reveals conduction slowing in connexin43 deficient mice**

Cardiovasc Res. 2001;51:681-690,

[Abstract](#) | [Full Text](#) | [PDF](#)

**Methods for Determining the Refractory Period and Excitable Gap During Persistent Atrial Fibrillation in the Goat**

Circulation. 2001;104:957-962,

[Abstract](#) | [Full Text](#) | [PDF](#)

**Optical measurement of cell-to-cell coupling in intact heart using subthreshold electrical stimulation**

Am. J. Physiol. Heart Circ. Physiol.. 2001;281:H533-H542,

[Abstract](#) | [Full Text](#) | [PDF](#)

**Mapping action potentials and calcium transients simultaneously from the intact heart**

Am. J. Physiol. Heart Circ. Physiol.. 2001;280:H2053-H2060,

[Abstract](#) | [Full Text](#) | [PDF](#)

**Pathophysiology and Prevention of Atrial Fibrillation**

Circulation. 2001;103:769-777,

[Full Text](#) | [PDF](#)

**Role of Structural Barriers in the Mechanism of Alternans-Induced Reentry**

Circ. Res.. 2000;87:1157-1163,

[Abstract](#) | [Full Text](#) | [PDF](#)

**Anisotropic Reentry in a Perfused 2-Dimensional Layer of Rabbit Ventricular Myocardium**

Circulation. 2000;102:2650-2658,

[Abstract](#) | [Full Text](#) | [PDF](#)

**Interdependence of Modulated Dispersion and Tissue Structure in the Mechanism of Unidirectional Block**

Circ. Res.. 2000;87:922-928,

[Abstract](#) | [Full Text](#) | [PDF](#)

**Ratiometry of transmembrane voltage-sensitive fluorescent dye emission in hearts**

Am. J. Physiol. Heart Circ. Physiol.. 2000;279:H1421-H1433,

[Abstract](#) | [Full Text](#) | [PDF](#)

**A Mechanism of Transition From Ventricular Fibrillation to Tachycardia : Effect of Calcium Channel Blockade on the Dynamics of Rotating Waves**

Circ. Res.. 2000;86:684-691,

[Abstract](#) | [Full Text](#) | [PDF](#)

**Spatiotemporal Heterogeneity in the Induction of Ventricular Fibrillation by Rapid Pacing : Importance of Cardiac Restitution Properties**

Circ. Res.. 1999;84:1318-1331,

[Abstract](#) | [Full Text](#) | [PDF](#)

**Mechanism Linking T-Wave Alternans to the Genesis of Cardiac Fibrillation**

Circulation. 1999;99:1385-1394,

[Abstract](#) | [Full Text](#) | [PDF](#)

**Mechanism of Acceleration of Functional Reentry in the Ventricle : Effects of ATP-Sensitive Potassium Channel Opener**

Circulation. 1999;99:704-712,

[Abstract](#) | [Full Text](#) | [PDF](#)

**Dispersion-based reentry: mechanism of initiation of ventricular tachycardia in isolated rabbit hearts**

Am. J. Physiol. Heart Circ. Physiol.. 1999;276:H413-H423,

[Abstract](#) | [Full Text](#) | [PDF](#)

**Modulated Dispersion Explains Changes in Arrhythmia Vulnerability During Premature Stimulation of the Heart**

Circulation. 1998;98:2774-2780,

[Abstract](#) | [Full Text](#) | [PDF](#)

**Role of Pectinate Muscle Bundles in the Generation and Maintenance of Intra-atrial Reentry : Potential Implications for the Mechanism of Conversion Between Atrial Fibrillation and Atrial Flutter**

Circ. Res.. 1998;83:448-462,

[Abstract](#) | [Full Text](#) | [PDF](#)

**Effects of Procainamide on Wave-Front Dynamics During Ventricular Fibrillation in Open-Chest Dogs**

Circulation. 1998;97:1828-1836,

[Abstract](#) | [Full Text](#) | [PDF](#)

**Characteristics of the Temporal and Spatial Excitable Gap in Anisotropic Reentrant Circuits Causing Sustained Ventricular Tachycardia**

Circ. Res.. 1998;82:279-293,

[Abstract](#) | [Full Text](#) | [PDF](#)

**Attachment of Meandering Reentrant Wave Fronts to Anatomic Obstacles in the Atrium : Role of the Obstacle Size**

Circ. Res.. 1997;81:753-764,

[Abstract](#) | [Full Text](#)

**Modulation of Ventricular Repolarization by a Premature Stimulus: Role of Epicardial Dispersion of Repolarization Kinetics Demonstrated by Optical Mapping of the Intact Guinea Pig Heart**

Circ. Res.. 1996;79:493-503,

[Abstract](#) | [Full Text](#)

**Characteristics of Wavefront Propagation in Reentrant Circuits Causing Human Ventricular Tachycardia**

Circulation. 2002;105:2172-2178,

[Abstract](#) | [Full Text](#) | [PDF](#)